High-energy diffuse scattering on the 1-ID beamline at the Advanced Photon Source

T. R. Welberry,[a]* D. J. Goossens,[a] D. R. Haeffner,[b] P. L. Lee[b] and J. Almer[b]

[a]Research School of Chemistry, Australian National University, Canberra, ACT 0200, Australia, and [b]Advanced Photon Source, Argonne National Laboratory, Argonne, IL, USA.
E-mail: welberry@rsc.anu.edu.au

This paper reports on experiments in which high-energy (65.35 keV) X-rays were used to record the detailed diffuse diffraction patterns of a number of ceramic materials. The methodology has enabled a greater **q**-range to be explored (up to $\sin\theta/\lambda \simeq 0.97$) than is possible with laboratory-based experiments, with better **q**-space resolution and increased sensitivity, thus allowing previously unseen detail in diffraction patterns to be recorded. In all, 11 sections of data have been collected for Ca-CSZ, eight for Y-CSZ and six for wüstite.

Keywords: diffuse scattering; cubic zirconia; wüstite; high-energy synchrotron radiation.

1. Introduction

Although diffuse scattering from a crystal can easily be observed by directing the incident beam onto a stationary crystal and recording the scattering on a two-dimensional detector, this scattering corresponds to a curved section through reciprocal space. There is much to be gained, from an interpretation and analysis point of view, by collecting data from plane sections of reciprocal space. One way to achieve this result is to collect large numbers of curved two-dimensional sections as the crystal orientation is varied systematically and to subsequently retrieve plane sections from the resulting full three-dimensional data set. Such a strategy involves an enormous quantity of data (see Estermann & Steurer, 1998; Weber *et al.*, 2001). As an alternative, we have developed a technique, using flat-cone Weissenberg geometry, which allows plane sections of data to be recorded directly (Osborn & Welberry, 1990). In a previous study (Butler *et al.*, 2000), we performed a prototype experiment on the SRI-CAT 1-ID beamline at the Advanced Photon Source to assess the viability of obtaining measurements of plane sections of diffuse scattering using a similar geometric setup.

In that experiment, the data for a whole reciprocal-space section were recorded on a single image plate (IP). The IP was translated continuously in a horizontal direction behind a vertical Weissenberg slit, with the motion being directly coupled to the rotation of the crystal about the crystal axis, ω. With the smallest feasible slit width of 0.5 mm, it was found that, while good resolution was obtained in the direction of the diffraction angle, ξ, insufficient resolution was obtained in the direction corresponding to ω [see Butler *et al.* (2000) for a diagram of the experimental setup]. One of the aims in the present experiment was to modify the method to achieve improved resolution in ω.

2. Methods and materials

Experiments were carried out on samples of the non-stoichiometric iron oxide wüstite, $Fe_{1-x}O$, and two different cubic stabilized zirconias: an yttria-stabilized zirconia (Y-CSZ) of composition $Zr_{0.61}Y_{0.39}O_{1.805}$ and a calcia-stabilized zirconia (Ca-CSZ) of composition $Zr_{0.875}Ca_{0.125}O_{1.875}$. These experiments used 65.35 keV X-rays ($\lambda = 0.1897$ Å).

After some experimentation, it was decided that the stationary crystal would be exposed at incremental ω steps of 0.25°, in order to obtain the desired improvement in the ω resolution. With a 0.5 mm slit placed in front of (and close to) the recording plate, a single exposure thus resulted in a 0.5 mm-wide line of data on the IP. Before the next exposure, the IP was translated normal to the slit length by 0.5 mm, so that each exposure resulted in an independent record on the IP with (virtually) no overlap. On one IP, 300 such exposures were recorded over a total width of 150 mm, and this measurement corresponded to a rotation of 75.0° in ω. To record the total 360° of ω rotation, five IPs were required. The IP was positioned 648 mm from the sample, resulting in a maximum accessible value of $\sin\theta/\lambda \simeq 0.97$.

Exposures were governed by incident-beam monitor counts rather than clock time. Each ω setting typically required a 5 s exposure, but this time varied with the state of the storage-ring current by up to a factor of two. Similarly, the time taken to expose a complete IP was ~25 min, but this time also varied by approximately a factor of two. For a complete section of data consisting of five IPs, ~2 h was required. A substantial fraction of the total time resulted from the need to enter the station and manually change the IP (note that an on-line IP system now alleviates this problem). In all, 11 layers of data were collected for Ca-CSZ, eight for Y-CSZ and six for wüstite.

Some problems were encountered when the data were analysed. First, the data on each IP varied significantly in intensity from one side to the other. This behaviour is undoubtedly due to differences in image decay time. When the IP was scanned (usually a few minutes after the final exposure), part of the image had been recorded up to 50 min earlier (the first exposure), while the most recent exposures had been recorded only 5 min earlier. To take account of these differences, a scale factor, which depended linearly on the distance across the IP, was used to correct the data. Because of the high symmetry (cubic) of the samples, symmetrically equivalent diffuse peaks were used to estimate the scales – something that may not always be possible.

The data also suffered from parasitic low-angle scattering, which we attribute to a combination of air scattering and scattering from the collimation slits and beam stop. Insufficient beam time precluded any serious attempts at the elimination of this scattering, and this must be a priority for any future experiments. The scattering was removed from the final data by subtracting an empirical background curve of the form $I_b = a\exp(-bx) + c\exp(-dx) + e$, where a, b, c, d and e are constants and x is the distance on the IP corresponding to the angle ξ. The values of the constants were estimated by fitting to the minimum values of intensity that occurred for any ω at each value of ξ.

Although the IP cassette was located reproducibly in the experimental setup, there were some variations in the position and orientation of the data on the scanned plate. The orientation was readily determined by consideration of the position of symmetry-related scattering peaks. However, no simple means was available to determine the position of the zero of the diffraction angle, and this position was determined by trial and error during the final conversion to reciprocal lattice coordinates from the Weissenberg coordinates of the raw data.

3. Results

The spatial resolution of the recorded data was much better than that obtained in the prototype experiment (Butler *et al.*, 2000) and now exceeds the resolution available from our own laboratory-based experiments. Two examples are presented.

Fig. 1(*a*) shows one section of the data for the Ca-CSZ sample. Although data out to $\sin\theta/\lambda \simeq 0.97$ were recorded, for clarity only data below $\sin\theta/\lambda = 0.67$ are shown.

The diffuse peaks that are seen extending in rows parallel to [110] and which occur in pairs straddling the dark lines indicated in Fig. 1(*a*) are of prime importance in understanding the disorder in CSZs. These lines originate from the local relaxations of the cations around the vacancy defects in the O-atom array. In a previous study (of Y-CSZ), we pointed out that the peak on the high-angle side of the dark line is invariably more intense than that on the low-angle side. We attributed this behaviour to the fact that, because Y and Zr have very similar scattering factors, most of the asymmetric scattering must originate from a third-order term in the basic scattering equation (Butler & Welberry, 1993). In the Ca-CSZ pattern shown, it is clear that, for the first pair of peaks, that on the low-angle side of the dark line is the more intense; for the second pair, the intensities are fairly similar, while, for the third pair, the asymmetry is reversed. This result occurs because, for Ca-CSZ, there is a first-order term in the diffraction equation, which dominates at low angles. Fig. 1(*b*) shows the intensity profile through the succession of these peaks and includes higher-angle data that are not shown in Fig. 1(*a*).

Fig. 2 shows examples taken from the data recorded for the wüstite sample. Fig. 2(*a*) shows the detail around the origin of reciprocal space, which was inaccessible in our laboratory experiments. This figure exhibits a symmetric motif of diffuse superlattice peaks, which is characteristic of the paracrystalline distribution of defect clusters that has been invoked to explain the features of the diffraction pattern of wüstite (Welberry & Christy, 1997). Fig. 2(*b*) shows the corresponding region around the 200 reciprocal lattice peak. The marked asymmetry of this figure is explained by the size-effect relaxation of the structure around the defect clusters. Fig. 2(*c*) shows the (*h k* 1.38) reciprocal section, which corresponds to the plane though the diffuse superlattice peaks on the high-angle side of the (*h k* 1) diffraction motifs. This pattern (and patterns recorded for the 0.38**c***, 0.62**c*** and 1.62**c*** sections) contains a level of detail in the very weak scattering that accompanies the superlattice peaks that has not previously been observed. Current models can explain the scattering shown in Figs. 2(*a*) and 2(*b*), but these new data are so far unexplained and present a challenge for future models that, if met, should lead to a deeper understanding of this complex material.

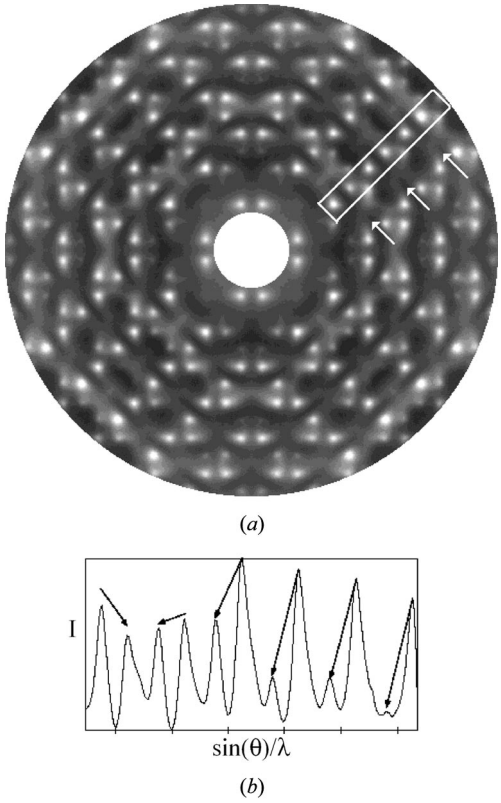

Figure 1
(*a*) The 0.5**c*** section of Ca-CSZ in the relatively low scattering-angle range $\sin\theta/\lambda \leq 0.67$. The 'dark lines' indicated by the arrows and the diffuse peaks enclosed in the white rectangle are referred to in the text. (*b*) The profile of the diffuse intensity along the [110] direction through these diffuse peaks (and including data extending out to $\sin\theta/\lambda \simeq 0.97$). The arrows indicate the asymmetry in intensity across the dark lines seen in (*a*).

4. Discussion

The present results indicate that the methodology described provides a viable means of extracting high-quality two-dimensional plane sections of diffuse-scattering data from disordered crystals. The use of high-energy X-rays has proved particularly effective for the highly absorbing materials investigated and has enabled a greater **q**-range to be explored (both low-**q** and high-**q**), as evidenced by Figs. 1(*b*) and 2(*a*). The penetration ability of high-energy X-rays allows us to study bulk structures without having to account for surface and absorption effects. We have achieved a **q**-space resolution that is significantly better than our best laboratory-based experiments. A much increased sensitivity has also been achieved, which allows, for example, the extra wüstite detail to be seen (Fig. 2*c*). This achievement is especially notable given that many further improvements to reduce the background are possible.

It is essential that future experiments address the question of low-angle parasitic scattering. The problem of the intensity gradient across the image will be overcome if a CCD detector is used instead

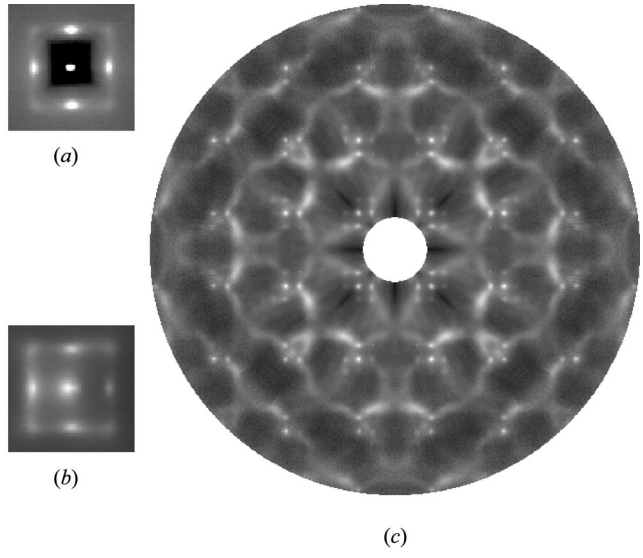

Figure 2
(*a*) The motif of diffuse superlattice peaks around the origin of reciprocal space of wüstite. (*b*) The asymmetric motif around the 200 reciprocal point. (*c*) The (*h k* 1.38) reciprocal section, which corresponds to the plane though the (weak) diffuse superlattice peaks on the high-angle side of the (*h k* 1) diffraction motifs.

of the IP. A CCD detector would also provide additional advantages in terms of automating the data collection.

We acknowledge the support of the Australian Synchrotron Research Program, reference No. 99/2000-SRI-40. The use of the Advanced Photon Source was supported by the US Department of Energy, Basic Energy Sciences, Office of Science, under contract No. W-31-109-Eng-38.

References

Butler, B. D., Haeffner, D. R., Lee, P. L. & Welberry, T. R. (2000). *J. Appl. Cryst.* **33**, 1046–1050.
Butler, B. D. & Welberry, T. R. (1993). *Acta Cryst.* A**49**, 736–743.
Estermann, M. A. & Steurer, W. (1998). *Phase Transit. B*, **67**, 165–195.
Osborn, J. C. & Welberry, T. R. (1990). *J. Appl. Cryst.* **23**, 476–484.
Weber, T., Estermann, M. A. & Bürgi, H.-B. (2001). *Acta Cryst.* B**57**, 579–590.
Welberry, T. R. & Christy, A. G. (1997). *Phys. Chem. Miner.* **24**, 24–38.